J Mater Sci: Mater Electron (2015) 26:6718–6722
DOI 10.1007/s10854-015-3275-x

Dielectric properties of microwave flash combustion derived and spark plasma sintered $CaCu_3Ti_4O_{12}$ ceramic: role of reduction in grain boundary activation energy

Ranjit Kumar[1,2] · M. Zulfequar[2] · T. D. Senguttuvan[1]

Received: 15 March 2015 / Accepted: 25 May 2015 / Published online: 3 June 2015

Abstract $CaCu_3Ti_4O_{12}$ nanocrystals have been synthesized by the microwave flash combustion technique. The calcined powders were spark plasma sintered at 1050 °C for 10 min. The surface morphology of sintered samples was studied by SEM. The effects of grain boundary activation energy on dielectric properties of CCTO were investigated by collecting the dielectric data in the frequencies of 30 Hz–8 MHz at temperatures of 20–100 °C under dc bias of 0–6 V. The potential energy barrier at grain boundary has been examined by dc bias experiments. It is observed that, with an increase in dc bias from 0 to 6 V, the grain boundary activation energy decreases from 0.532 to 0.463 eV. The reduction in such grain boundary activation energy results in the decrease in dielectric constant. It is noticed that CCTO ceramic at room temperature under zero dc bias has a colossal dielectric constant of 20,000 (at 100 Hz). Using the cole–cole plot, grain and grain boundary resistance are calculated to be 13 and 52,100 Ω, respectively.

1 Introduction

$CaCu_3Ti_4O_{12}$ (CCTO), a colossal dielectric constant (CDC) material, is one of the best candidates for ultra-miniaturization of energy storage electronic devices. CCTO presenting a huge dielectric constant ($>10^4$) and good stability over a wide temperature range (100–500 K). It has a body-centered cubic perovskite-like structure (space group of *Im*3) with slightly tilted TiO_6 octahedron. The tilted TiO_6 octahedron arises due to the share of different size of cations (Ca^{+2} and Cu^{+2}) at A site and the bound of Cu^{+2} ions to four oxygen atoms in square planar environment [1–8].

Some researchers suggested that the anomalous dielectric behaviour of CCTO is based on intrinsic effects (perfectly stoichiometric, defect-free and single-domain) [1, 3], while other have attributed to extrinsic effects (defects, domain boundaries, Cu rich grain boundaries, nanoscale disorder, electrode polarization, bimodal grain distribution, Schottky-type barriers at grain boundary, thermally active dielectric relaxation, lattice distortion, and inter barrier layer capacitance) [4–12]. However, an extrinsic effect: inter barrier layer capacitance which based on semiconducting grains and insulating grain boundary is widely accepted. A microstructure having semiconducting grains and insulating grain boundary can be grown by adjusting the processing conditions of synthesis [13–16].

Initially, CCTO was synthesized by the solid state reaction route. Recentally, various new synthesis techniques have been employed to synthesize CCTO. These techniques have reduced processing time and temperature, and enhanced its dielectric properties. Some of the reported synthesis technique are sol–gel [13], polymerized complex method [14], coprecipitation [15], wet-chemical synthesis using nitrate and organometallic salts [16], polymeric citrate precursor method [17], pyrolysis of organic solution [18], microwave calcination of oxide powders [19], molten salt method [20], etc. Many of them have produced the nanoparticle of CCTO.

In recent years, a new synthesis technique known as microwave flash combustion technique is used to

✉ Ranjit Kumar
krranajeet@gmail.com

[1] Physics of Energy Harvesting Division, National Physical Laboratory (CSIR), Dr. K.S. Krishnan Marg, New Delhi 110012, India

[2] Department of Physics, Jamia Millia Islamia, Jamia Nagar, New Delhi 110025, India

synthesize the nanomaterials. It produces high purity, stoichiometric and crystalline nanomaterial. This technique is fundamentaly different from other synthesis technique as the heat is generated at molecular level and the reaction is exothermic, self-sustaining and rapid. In this technique, an aqueous solution of mixture of the precusors and the fuel is irradiated with microwave power. During the microwave irradiation, solution is subjected to a varying electromagnetic field, which causes the conduction of free charges and re-orientation of dipoles. The permanent dipoles try to orient itself with field oscillation, but they could not cope up because of inter molecular force and molecular inertia. This causes a phase lag that results in power absorbed in the form of heat through molecular friction and dielectric loss. The microwave power (P) absorbed per unit volume (W/m^3) is given as $P = \sigma |E|^2 = 2\pi f \varepsilon_o \varepsilon' \tan\delta |E|^2$, where σ is conductivity, E is electric field, f is frequency, ε_o is permittivity of free space, ε' is dielectric constant and $\tan\delta$ is a loss factor. The aqueous solution in this technique contains the metal nitrates as oxidant and a suitable organic compound such as urea, citric acid, oxalic acid, glycene, hydrazine and L-alanine as fuel. The solution combusted by microwave provides the enhanced reaction kinetics, thus improves the yield and reduces the processing time. Using this method, oxide nanomaterial such as MgO [21], TiO_2 [22], Nd:Y_2O_3 [23], NiO-YSZ [24], $CdFe_2O_4$ [25], Ti-substituted Zn ferrite [26] and others have been synthesized. Recently, we have synthesized nanocrystalline $CaCu_3Ti_4O_{12}$ ceramic for the first time by the microwave flash combustion method [5].

In this work, nanocrystalline CCTO powders have been synthesized by the microwave flash combustion technique. The powders were sintered by spark plasma sintering. The role of reduction in grain boundary activation energy on dielectric properties has been studied.

2 Experimental

$CaCu_3Ti_4O_{12}$ nanopowders were synthesized by the microwave flash combustion technique. The detail about this synthesis was described in our previous report [5]. Briefly, aqueous solution containing $Ca(NO_3)_2{\cdot}4H_2O$, $Cu(NO_3)_2{\cdot}4H_2O$ and $TiO(NO_3)_2$ as oxidizers and CH_4N_2O (urea) as a fuel was irradiated with microwave power (2.45 GHz and 1.1 kW). An oxidant-to-fuel (O/F) ratio or equivalent ratio (φ_e) was taken as 1. The synthesized CCTO nonoparticles after combustion were calcinated at 900 °C for 5 h.

The calcined powders were spark plasma sintered at 1050 °C for 10 min under an uniaxial pressure of 50 MPa using a DR. SINTER SPS-725 system. Sintered pellet having diameter of 15 mm and thickness of 2.3 mm were obtained. Graphite die was used for making the pellets during sintering. The microstructure and surface morphology of sintered samples were studied by scanning electron microscope (Zeiss EVO MA 10). Dielectric properties of sintered pellets were measured using an impedance analyzer (Alpha-A, Novacontrol high frequency analyzer). The dielectric data were collected in a frequency range of 30 Hz–8 MHz, a bias voltage of 0–6 V, and a temperature range of 20–100 °C. Dielectric measurements were carried out by making the sintered pellets as a parallel plate capacitor using silver electrodes fired at 500 °C.

3 Results and discussion

3.1 Structural analysis

XRD and TEM measurements of CCTO nanoparticles synthesized by microwave flash combustion technique are in accordance with the our previous work [5]. In the previous work, we have demostrated that XRD patterns of CCTO synthesized by microwave flash combustion technique are match well with a body-centered cubic perovskite-like CCTO structure of cell parameter of 7.38 Å (JCPDF file no. 010752188). From TEM measurements, we have also obseved that average particle size were in the range of 50–70 nm. In the present work, Fig. 1 shows the SEM micrograph of CCTO pellets sintered at 1050 °C for 10 min using spark plasma sintering. Using this sintering method, highly dense CCTO microstructure has been obtained as the heat is generated for sintering is due to simultaneous application of mechanical pressure and high-power pulse. A dense CCTO microstructure has well developed grain and grain boundary. The average grain size is measured to be 2 μm and density is calculated to be 98 % of theoretical density.

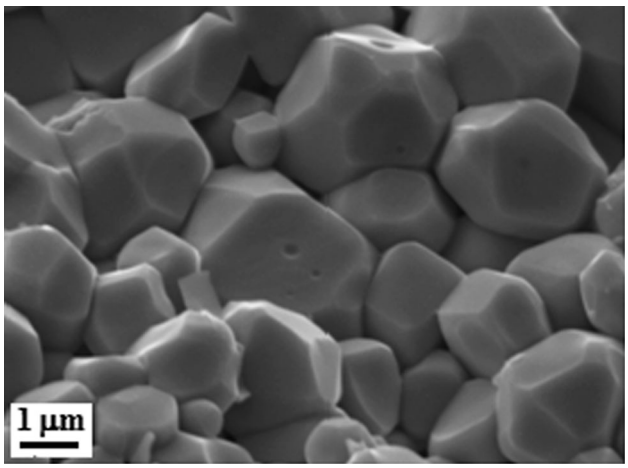

Fig. 1 SEM image of CCTO pellets sintered at 1050 °C for 10 min using spark plasma sintering

3.2 Dielectric properties and impedance specroscopic studies

Frequency dependence of the real part of dielectric permittivity (ε′-dielectric constant), measured under 0–6 V dc bias, of sintered sample is shown in Fig. 2. Figure 2 reveals that CCTO samples measured under zero bias have a colossal dielectric constant of ∼20,000 at 100 Hz. This figure shows that the dielectric constant gradually increased with decrease in frequency, but it gradually decreased with increase in dc bias voltage. This effect is seen prominently at low frequencies (<1 kHz). The decrease of dielectric constant in the high frequency region (>1 kHz) is due to a transition from grain dielectric response to grain boundary dielectric response. The decrease in dielectric constant with an increase in dc bias voltage is associated with the decrease in capacitance of grain boundary. Guo et al. [27] and Adams et al. [28] have demonstrated that the capacitance of CCTO grain boundaries decreases with increasing dc bias. Such grain boundary based dielectric constant behaviour has been detected by impedance spectroscopy.

Impedance spectroscopic Z* plot (cole–cole plot) of the same dielectric data is shown in Fig. 3. The observed cole–cole plots for 0, 2, 4 and 6 V dc bias are in the semicircular arc. The inset of Fig. 3 shows that the semicircles are not originating from the origin. Since it is not originated from origin, the observed semicircles are associated with grain boundary as suggested by impedance spectroscopy. Using these non zero intercepts on Z′ axis the grain resistance (R_g) and the grain boundary resistance (R_{gb}) have been calculated. The values of R_g and R_{gb} with zero dc-bias are 13 and 52,100 Ω, respectively. It is noticed that the resistance of grain boundary decreases substantially with an increase of bias voltage as the intercepts on Z′ axis move toward origin. Similar effects were observed in other reports [27–29]. However, the grain resistance remains almost same. The increase in grain boundary conductivity ($\sigma_{gb} = 1/R_{gb}$) with an increase in dc- bias voltage is shown in Fig. 4. It is clear from this figure that the conductivity showing a non-linear I–V response. This response presents that CCTO grain boundary having non-Ohmic electrical properties. The non-Ohmic electrical response of grain boundary indicates that there is an existence of diode-like back-to-back Schottky barriers. This is consistent with report [3, 27–30]. These reports suggest that such barriers are created due to charge trapping of accepter states at the interfaces between two adjacent n-type grains with insulating grain boundary (semiconductor-insulator-semiconductor structure, where $R_b \ll R_{gb}$). When the bias voltage is applied to the back-to-back Schottky diode between two

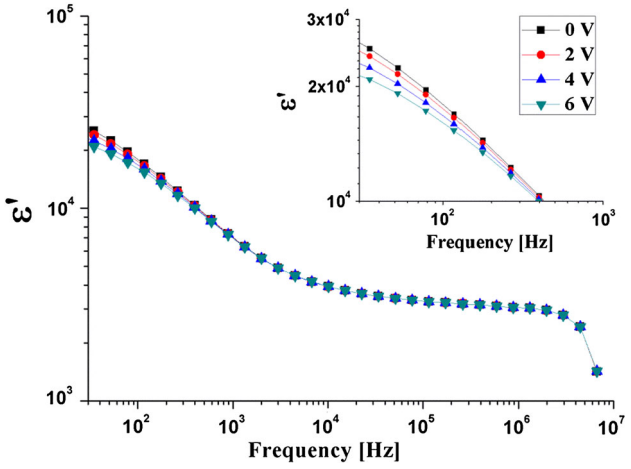

Fig. 2 Frequency dependent of the dielectric constant, measured under zero dc bias, of sintered CCTO samples. The *inset* shows an extrapolated graph at low frequencies region

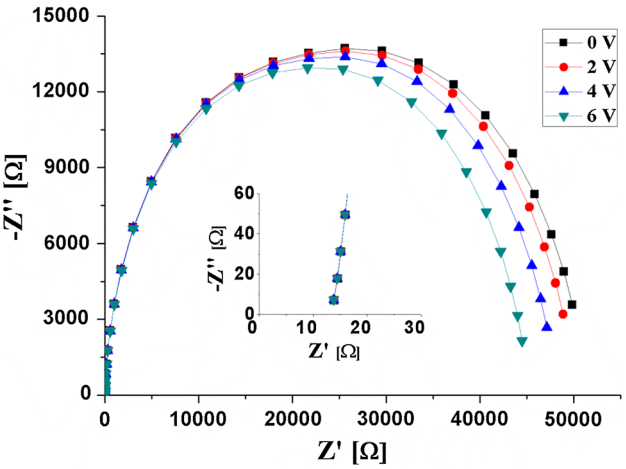

Fig. 3 Cole–cole plot of sintered CCTO sample obtained under a dc bias of 0, 2, 4 and 6 V. The *inset* shows an extrapolated graph near to origin

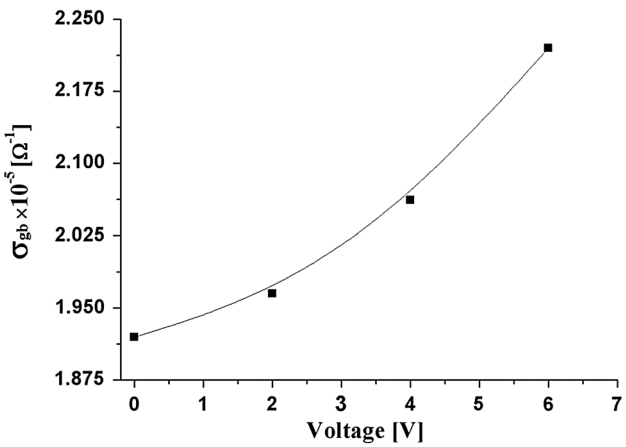

Fig. 4 Variation of grain boundary conductivity with applied dc bias voltage

adjacent CCTO grains, one of the Schottky diode is forward biased (semiconductor-insulator structure) while other is reverse biased (insulator-semiconductor structure). Forward bias band reduces the depletion contribution while reverse bias band enhances the depletion contribution. Under the non-ohmic applied bias voltage, the amount of shrinkage and extension of depletion region in forward and reverse side are unequal as forward side pins and reverse side keeps extending by dropping the voltage. This results in an increase of total width of depletion region. An increase of the width of depletion region causes the decrease in grain boundary capacitance. Further, the Schottky diode like electrical barriers at grain boundary has a potential energy barrier height which restricts the motion of mobile charge carriers. Since, the motion of mobile charge carriers is thermally activated process also. Therefore, the height of potential energy barriers can be measured in terms of activation energy [28, 31].

The activation energy of grain boundary has been calculated by collecting the cole–cole plots, under 0 V bias, in the temperature range of 20–100 °C (Fig. 5). It is evident from figure that an increase in measuring temperature both the grain and grain boundary resistance decreased, and the frequency at the peak of semicircles (f_{max}) increased. The increase of f_{max} with increase in temperature follows the Arrhenius law. Using Arrhenius equation ($f_{max} = f_o\ exp\ (-E_a/k_BT)$), where the symbols have their usual meaning, activation energy has been calculated. It was notice that under 2, 4 and 6 V bias, the increase of f_{max} follows the Arrhenius law (not shown). The calculated grain boundary activation energies (E_a) at 0, 2, 4 and 6 V are shown in Fig. 6. Figure 6 shows that with an increase in dc-bias voltage the activation energy of grain boundary decreases from 0.532 to 0.463 eV. The decrease in the activation energy with an increase in dc-biasing is associated with the

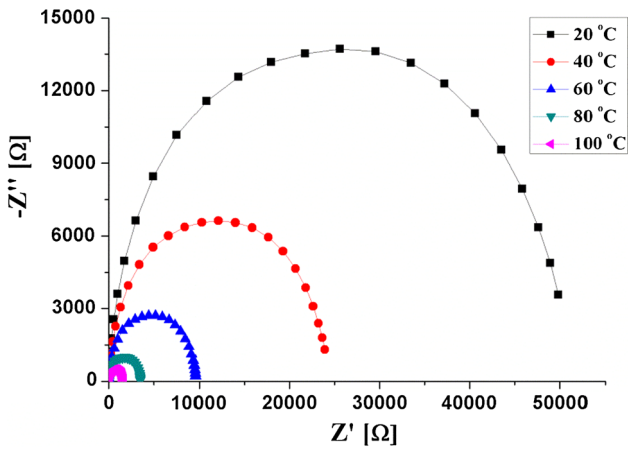

Fig. 5 Cole–cole plot of sintered CCTO sample obtained under zero dc bias at temperatures of 20–100 °C

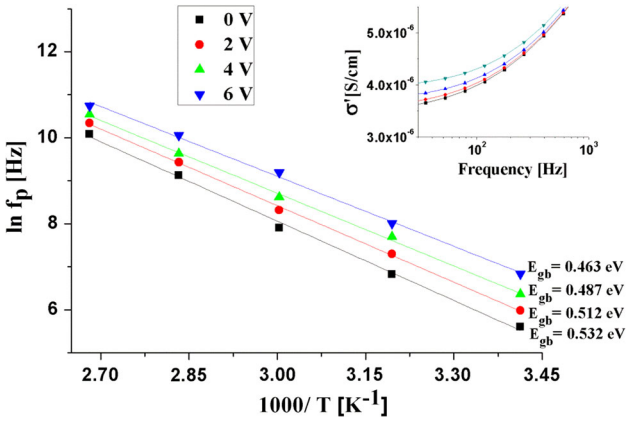

Fig. 6 Arrhenius plot for the activation energy of grain boundary obtained under a dc bias of 0, 2, 4 and 6 V. The *inset* shows the frequency dependence of the real part of conductivity. The *inset* shows the real part of conductivity in the low frequencies (<1000 Hz) at room temperature

reduction in the potential energy height of Schottky barrier. The reduction in potential energy of Schottky barriers leads to the increase in width of depletion zone, which results in the decrease in the capacitance of grain boundary [28, 30–37]. This effect is seen in Fig. 4 where permittivity of CCTO is decreases with increase in dc bias voltage. The reduction in potential barrier height with increase in dc biasing has been also be noticed by an increase in real part conductivity (σ') [inset of Fig. 6]. Figure 6 shows that conductivity increases with an increase in biasing as the motion of charge carriers possess low restriction. From above observed data, it is clear that the presence of potential barrier at insulating grain boundary forms an inter barrier layer capacitor (IBLC) between conducting grains. This results in the detection of very large values of dielectric permittivity.

4 Conclusion

Nanocrystalline $CaCu_3Ti_4O_{12}$ ceramic has been derived from microwave flash combustion technique. The calcined CCTO nanoparticles were spark plasma sintered at 1050 °C for 10 min under an uniaxial pressure of 50 MPa. Sintered sample has the average grain size of 2 μm and density of 98 %. The dc bias measurement shows that grain boundary have a potential-energy barrier which gives rise to a non-ohmic electrical property. It is found that, with an increase in dc bias, the grain boundary activation energy has been reduced which results in the decrease in dielectric constant. This result supports that the CCTO ceramic display an inter barrier layer capacitance behavior. The electrical properties of CCTO ceramic, at room temperature under zero dc bias, shows that it has a colossal dielectric

constant of 20,000 (at 100 Hz), grain resistance of 13 Ω and grain boundary resistance of 52,100 Ω.

Acknowledgments Ranjit Kumar is thankful to the Council of Scientific and Industrial Research (CSIR), New Delhi for award of research fellowship.

References

1. M.A. Subramanian, D. Li, N. Duan, B.A. Reisner, A.W. Sleight, J. Solid State Chem. **151**, 323 (2000)
2. C.C. Homes, T.S. Vogt, M. Shapiro, S. Wakimoto, A.P. Ramirez, Science **293**, 673 (2001)
3. S.Y. Chung, I.D. Kim, S.L. Kang, Nat. Mater. **3**, 774 (2004)
4. D.C. Sinclair, T.B. Adams, F.D. Morrison, A.R. West, Appl. Phys. Lett. **80**, 2153 (2002)
5. R. Kumar, M. Zulfequar, L. Sharma, V.N. Singh, T.D. Senguttuvan, Cryst. Growth Des. **15**, 1374 (2015)
6. R. Kumar, M. Zulfequar, V.N. Singh, J.S. Tawale, T.D. Senguttuvan, J. Alloys Compd. **541**, 428 (2012)
7. Z. Xu, H. Qiang, Z. Chen, Y. Chen, J. Mater. Sci. Mater. Electron. **26**, 578 (2015)
8. A.M. Awasthi, J. Kumar, J. Appl. Phys. **112**, 54108 (2012)
9. J. Zheng, A.I. Frenkel, L. Wu, J. Hanson, W. Ku, E.S. Bozin, S.J.L. Billinge, Y. Zhu, Phys. Rev. B **81**, 144203 (2010)
10. M.A. Rubia, P. Leret, J. Frutos, J.F. Fernandez, J. Am. Ceram. Soc. **95**, 1866 (2012)
11. J.F. Fernandez, P. Leret, J.J. Romero, J. Frutos, M.A. Rubia, M.S. Gonzalez, J.L. Kramer, J.L.G. Fierro, A. Quesada, M.A. Garcia, J. Am. Ceram. Soc. **92**, 2311 (2009)
12. P. Delugas, P. Alippi, V. Fiorentini, V. Raineri, Phys. Rev. B **81**, 81104 (2010)
13. R. Parra, E. Joanni, J.W.M. Espinosa, R. Tararam, M. Cilense, P.R. Bueno, J.A. Varela, E. Longo, J. Am. Ceram. Soc. **91**, 4162 (2008)
14. C. Masingboon, P. Thongbai, S. Maensiri, T. Yamwong, S. Seraphin, Mater. Chem. Phys. **109**, 262 (2008)
15. B. Barbier, C. Combettes, S.G. Fritsch, T. Chartier, F. Rossignol, A. Rumeau, T. Lebey, E. Dutarde, J. Eur. Ceram. Soc. **29**, 731 (2009)
16. W.X. Yuan, Z.J. Li, Eur. Phys. J. Appl. Phys. **57**, 11302 (2012)
17. P. Jha, P. Arora, A.K. Ganguli, Mater. Lett. **57**, 2443 (2003)
18. J. Liu, Y. Sui, C. Duan, W.N. Mei, R.W. Smith, J.R. Hardy, Chem. Mater. **18**, 3878 (2006)
19. H. Yu, H. Liu, D. Luo, M. Cao, J. Mater. Process. Technol. **208**, 145 (2008)
20. K.P. Chen, Y. He, D.Y. Liu, Z.D. Liu, Key Eng. Mater. **368–372**, 115 (2008)
21. S. Makhluf, R. Dror, Y. Nitzam, Y. Abramovich, R. Jelinek, A. Gedanken, Adv. Funct. Mater. **15**, 1708 (2005)
22. T.V. Anuradha, S. Ranganathan, Bull. Mater. Sci. **30**, 263 (2007)
23. M. Rekha, K. Laishram, R.K. Gupta, N. Malhan, A.K. Satsangi, J. Mater. Sci. **44**, 4252 (2009)
24. H. Mohebbi, T. Ebadzadeh, F.A. Hesari, Powder Technol. **188**, 183 (2009)
25. V. Vasanthi, A. Shanmugavani, C. Sanjeeviraja, R.K. Selvan, J. Magn. Magn. Mater. **324**, 2100 (2012)
26. P.P. Hankare, R.P. Patil, A.V. Jadhav, R.S. Pandav, K.M. Garadkar, R. Sasikala, A.K. Tripathi, J. Alloys Compd. **509**, 2160 (2011)
27. M. Guo, T. Wu, T. Liu, S.X. Wang, X.Z. Zhao, J. Appl. Phys. **99**, 124113 (2006)
28. T.B. Adams, D.C. Sinclair, A.R. West, Phys. Rev. B **73**, 94124 (2006)
29. C. Mu, H. Zhang, Y. He, J. Shen, P. Liu, J. Phys. D Appl. Phys. **42**, 175410 (2009)
30. I. Kim, A. Rothschild, H.L. Tuller, Appl. Phys. Lett. **88**, 72902 (2006)
31. L. Liu, H. Fan, P. Fang, X. Chen, Mater. Res. Bull. **43**, 1800 (2008)
32. P.R. Emtage, J. Appl. Phys. **48**, 4372 (1977)
33. P. Liu, Y. He, J. Zhou, C. Mu, H. Zhang, Phys. Status Solidi A **206**(3), 562 (2009)
34. M.A. Alim, S. Li, F. Liu, P. Cheng, Phys. Status Solidi A **203**(2), 410 (2006)
35. F. Iguchi, C. Chen, H. Yugami, S. Kim, J. Mater. Chem. **21**, 16517 (2011)
36. P.R. Bueno, J.A. Varela, E. Longo, J. Eur. Ceram. Soc. **28**, 505 (2008)
37. T.T. Fang, H.K. Shiau, J. Am. Ceram. Soc. **87**, 2072 (2004)